applied optics

Effect of a codoped interface layer on passively Q-switched laser performance of composite crystals

JIE XU AND JUN DONG*

Department of Electronics Engineering, School of Information Science and Engineering, Xiamen University, Xiamen 361005, China
**Corresponding author: jdong@xmu.edu.cn*

Received 17 May 2016; revised 14 July 2016; accepted 21 July 2016; posted 22 July 2016 (Doc. ID 265490); published 10 August 2016

By using combinations of appropriate laser crystals, we simulated a Yb:YAG/Cr^{4+}:YAG composite crystal with a Cr,Yb:YAG interface layer. The effect of the Cr,Yb:YAG interface layer on the laser performance of the Yb:YAG/Cr^{4+}:YAG composite crystal has been investigated for the first time to our best knowledge. The formation of the Cr,Yb:YAG interface layer in the Yb:YAG/Cr^{4+}:YAG composite crystal has a negative impact on average output power, optical efficiency, as well as single pulse energy and peak power. In addition, the Cr,Yb:YAG interface layer also leads to strong mode competition, resulting in the decrease of the longitudinal mode number, the widening of longitudinal mode separations, and the poor stability of laser pulse trains. The results of this study are of theoretical and practical importance to develop novel Yb:YAG/Cr^{4+}:YAG composite crystals that could be used to obtain laser pulses with high peak power and high optical efficiency.

OCIS codes: (140.3540) Lasers, *Q*-switched; (140.3580) Lasers, solid-state; (160.3380) Laser materials; (160.4760) Optical properties.

http://dx.doi.org/10.1364/AO.55.006516

1. INTRODUCTION

Laser diode pumped passively *Q*-switched lasers can obtain laser pulses with high beam quality and high peak power so they have wide applications in laser processing, laser range finders, engine ignitions, remote sensing and environmental pollution detection, and so on. Therefore, development of high peak power passively *Q*-switched microchip lasers has become a hot issue in the solid-state laser field. Passively *Q*-switched microchip solid-state lasers are usually constructed with separated gain medium and the saturable absorber. There is an air gap between gain medium and saturable absorber, which increases the difficulty of the thermal transfer between them. On the other hand, air breakdown occurs on the contact face when the passively *Q*-switched microchip laser works at a peak power of >100 kW or 1 MW. The coatings on surfaces of a gain medium or saturable absorber are damaged, which strongly affects the performance of the passively *Q*-switched microchip laser. Composite laser materials fabricated by thermal bonding techniques have been demonstrated to mitigate the thermal problem and eliminate the air gap between the gain medium and saturable absorber for high peak power passively *Q*-switched microchip lasers. Diffusion-bonded composite crystals have resulted in the reduction of peak temperature rise in the active region and the alleviation of the thermal lensing effect [1], which is a benefit for high power laser operation. Composite laser materials have been widely used in constructing compact passively *Q*-switched miniature lasers with high optical-to-optical efficiency and high peak power. A laser diode pumped Nd:YAG/Cr^{4+}:YAG composite crystal passively *Q*-switched microchip laser has been demonstrated with pulse width of 337 ps for the first time to the best of our knowledge [2]. A Yb:YAG/Cr^{4+}:YAG composite ceramics picosecond passively *Q*-switched microchip laser with a peak power of 0.72 MW has been achieved [3]. A composite, all-ceramic, high peak power Nd:YAG/Cr^{4+}:YAG monolithic microlaser for engine ignition has been demonstrated [4]. A Yb:YAG/Cr^{4+}:YAG composite crystal passively *Q*-switched laser with an optical-to-optical efficiency of 36% and a slope efficiency of 44% has also been achieved [5]. A comparison between thermally bonded and unbonded Er^{3+}, Yb^{3+}:glass/Co^{2+}:$MgAl_2O_4$ microchip lasers has revealed a considerable improvement in the peak power and efficiency due to lower internal loss in thermally bonded crystals as well as threshold reduction. Mode competition has also been observed in the unbonded Er^{3+}, Yb^{3+}:glass/Co^{2+}:$MgAl_2O_4$ sample [6]. Therefore, composite crystals based on various gain medium and saturable

absorbers have been widely used in constructing highly efficient, high peak power passively Q-switched microchip lasers for various applications.

However, there is an interface layer through ion diffusion between the gain medium and the saturable absorber in the composite materials fabricated with a thermal bonding technique. The thickness of the interface layer of composite materials depends on the temperature and pressure used in the fabrication process. Taking Yb:YAG/Cr^{4+}:YAG composite crystal as an example, the Yb^{3+} ions are diffused into the Cr:YAG part, and the Cr^{4+} ions and other related ions in the Cr^{4+}:YAG part are diffused into the Yb:YAG part during the thermal bonding process. Therefore, a Cr,Yb:YAG interface layer with varying ion concentrations is formed at the interface of the Yb:YAG/Cr^{4+}:YAG composite crystal. Although Cr,Yb:YAG codoped materials have been demonstrated to be self-Q-switched laser materials [7] and self-Q-switched microchip lasers have been demonstrated [8], the fluorescence lifetime of Cr,Yb:YAG decreases with the Cr^{4+} ions doping concentration, and more defects are introduced in Cr,Yb:YAG self-Q-switched laser materials [9]. Cr^{4+} ions have a broad absorption band from 900 to 1200 nm, and the efficient absorption of pump power from a 940 nm laser diode is degraded owing to the absorption of Cr^{4+} ions at 940 nm. The self-absorption effect at a laser wavelength of 1030 nm of Cr,Yb:YAG crystals is more serious than that of Yb:YAG crystals [10]. The fluorescence lifetime of Cr,Yb:YAG crystals is only 61% of the fluorescence lifetime of Yb:YAG crystals when the Cr ions doping concentration is 0.025 at. % [9,11]. Moreover, the lattice distortions in Cr,Yb:YAG crystals are getting severe with the increase of Cr^{4+} ion doping concentration, so it is more difficult to transfer heat through lattice vibrations. Besides Yb^{3+} ions and Cr^{4+} ions, there are many other doping ions in a Cr,Yb:YAG crystal. Cr^{4+} ions in Cr,Yb:YAG crystals have more than one valence state, and Cr^{4+} ions are only a very small fraction of Cr ions. Moreover, Mg^{2+} ions or Ca^{2+} ions were added into Cr,Yb:YAG crystals as compensate charges. In a Cr,Yb:YAG crystal, Yb^{3+} ions take the place of some Y^{3+} ions; Cr^{3+} ions and Cr^{4+} ions replace some Al^{3+} ions; and Mg^{2+} ions and Ca^{2+} ions take the place of some Al^{3+} ions and Y^{3+} ions. The radii of some ions [12] are shown in Table 1.

Although the radii of Yb^{3+} ions are comparable to that of Y^{3+} ions in YAG, the radii of the Cr^{3+} ions, Cr^{4+} ions and Ca^{2+} compensator ions are much larger than that of the Al^{3+} ions they replaced. As a result, the lattice distortions in Cr,Yb:YAG crystals become severe with the increase of Cr^{4+} ion doping concentration. Therefore, the Cr,Yb:YAG interface layer formed in Yb:YAG/Cr^{4+}:YAG composite crystals must have a strong effect on the performance of Yb:YAG/Cr^{4+}:YAG composite crystals passively Q-switched microchip laser. However, there are not any reports on the effect of Cr,Yb:YAG interface layer on the performance of Yb:YAG/Cr^{4+}:YAG composite crystal passively Q-switched lasers.

Table 1. Radii of Some Ions in Cr,Yb:YAG Crystals

Name of Ions	Radius/nm
Ca^{2+}	0.10
Al^{3+}	0.053
Cr^{3+}	0.0615
Cr^{4+}	0.055
Y^{3+}	0.1015
Yb^{3+}	0.098

In this paper, the effects of the Cr,Yb:YAG interface layer on the performance of Yb:YAG/Cr^{4+}:YAG composite crystal have been investigated by sandwiching a Cr,Yb:YAG codoped crystal between the Yb:YAG and Cr^{4+}:YAG crystal. The performance of Yb:YAG/Cr, Yb:YAG/Cr^{4+}:YAG passively Q-switched microchip laser has been investigated and compared to the Cr^{4+}:YAG passively Q-switched microchip laser and Yb:YAG enhanced Cr,Yb:YAG self-Q-switched microchip laser.

2. STRUCTURE OF Yb:YAG/Cr^{4+}:YAG COMPOSITE CRYSTAL

The thermal bonding technique is also called the thermal diffusion bonding technique, which is a process that can bond two separated crystals together by using the thermal diffusion effect. In general, Yb:YAG/Cr^{4+}:YAG composite crystals are usually made by the thermal bonding technique. The distributions of Yb^{3+} ions and Cr^{4+} ions before and after the thermal bonding process are shown in Fig. 1. During the thermal diffusion bonding process, Yb^{3+} ions in a Yb:YAG crystal are diffusing into the Cr^{4+}:YAG crystal; at the same time, Cr^{4+} ions in a Cr^{4+}:YAG crystal are diffusing into the Yb:YAG crystal. Therefore, a codoped Cr,Yb:YAG interface layer is formed at the interface of the Yb:YAG and Cr^{4+}:YAG crystals. The doping concentrations of Yb^{3+} ions and Cr^{4+} ions along the diffusion distances are not uniform after the thermal diffusion process, as shown in Fig. 1. The doping concentrations of Yb^{3+} ions and Cr^{4+} ions decrease with their diffusion distances, which is similar to that in Nd:YAG/YAG transparent ceramics [13] and YAG/Yb:YAG composite ceramics [14]. The doping concentrations of Yb^{3+} ions and Cr^{4+} ions can be calculated by the following equation [15]:

$$C(t,x) = \frac{C_0}{2}\,\mathrm{erfc}\left(\frac{x-x_0}{2\sqrt{Dt}}\right) \tag{1}$$

and the boundary condition is

$$C(t=0,x) = \begin{cases} C_0 (x \le x_0) \\ 0 (x \ge x_0) \end{cases}, \tag{2}$$

where C_0 is the initial concentration of ions, and D is the diffusion coefficient, which is related to the temperature used in the thermal diffusion bonding process. x is the coordinate for the diffusion direction, and x_0 is the boundary coordinate. t is

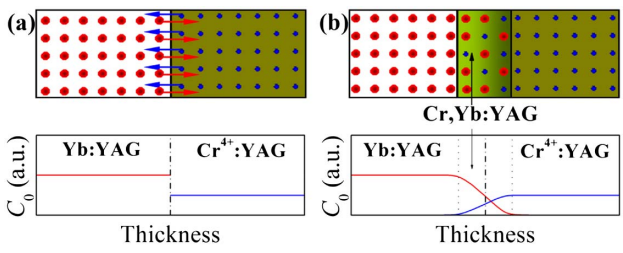

Fig. 1. Distribution of Yb^{3+} ions and Cr^{4+} ions (a) before and (b) after the thermal bonding process.

Table 2. Three Different Combinations of Yb:YAG, Cr,Yb:YAG, and Cr^{4+}:YAG Crystals

Serial Number	Combination of Crystals	Thickness of Cr,Yb:YAG Interface Layer
C1	Yb:YAG + Cr^{4+}:YAG	0
C2	Yb:YAG + Cr, Yb:YAG	Equal to the thickness of the Cr^{4+}:YAG part in Yb:YAG/Cr^{4+}:YAG
C3	Yb:YAG + Cr, Yb:YAG + Cr^{4+}:YAG	Relatively moderate

the diffusion time. The diffusion distance of the doping ions concentration depends on the temperature and time used in thermal bonding process. The Cr^{4+} ion doping concentration of the Cr,Yb:YAG interface layer increases with the Cr^{4+} ion doping concentration of the Cr^{4+}:YAG part in the Yb:YAG/Cr^{4+}:YAG composite crystal.

In general, a Cr^{4+}:YAG saturable absorber with low initial transmission is needed in a Yb:YAG/Cr^{4+}:YAG composite crystal passively *Q*-switched laser for high peak power generation. For this laser, a thin Cr^{4+}:YAG crystal with a high doping concentration for achieving a low initial transmission is desirable. However, a highly doped Cr^{4+}:YAG crystal results in strong variation of the Cr^{4+} ions and more defects and distortion in the Cr,Yb:YAG interface layer. Although the thickness of the Cr,Yb:YAG interface layer in the Yb:YAG/Cr^{4+}:YAG composite crystal is not long (<100 μm) [13,15], the variation of the Yb^{3+} ions and Cr^{4+} ions in the Cr,Yb:YAG interface layer has a great effect on the laser performance of the Yb:YAG/Cr^{4+}:YAG composite crystal. Therefore, the effect of the Cr,Yb:YAG interface layer on the performance of the Yb:YAG/Cr^{4+}:YAG composite crystal should be considered.

The Yb:YAG/Cr^{4+}:YAG composite crystal fabricated by thermal bonding technology can be considered as a combination of Yb:YAG, Cr,Yb:YAG, and Cr^{4+}:YAG crystals. A Cr, Yb:YAG crystal with appropriate thickness and doping concentration is used to be an equivalence of the Cr,Yb:YAG interface layer in a Yb:YAG/Cr^{4+}:YAG composite crystal. Therefore, three different combinations of separated Yb:YAG, Cr,Yb:YAG, and Cr^{4+}:YAG crystals were used to investigate the effect of the Cr,Yb:YAG codoped interface layer on the passively *Q*-switched laser performance of the Yb:YAG/Cr^{4+}:YAG composite crystal. Yb:YAG and Cr^{4+}:YAG crystals were used to simulate the Yb:YAG/Cr^{4+}:YAG composite crystal without a Cr,Yb:YAG interface layer. Yb:YAG and Cr,Yb:YAG crystals were used to simulate a Yb:YAG/Cr^{4+}:YAG composite crystal with a Cr, Yb:YAG interface layer whose thickness is equal to the thickness of the Cr^{4+}:YAG part in the Yb:YAG/Cr^{4+}:YAG composite crystal. Yb:YAG, Cr,Yb:YAG, and Cr^{4+}:YAG crystals were used to simulate the Yb:YAG/Cr^{4+}:YAG composite crystal with a Cr,Yb:YAG interface layer. The three combinations of Yb:YAG, Cr,Yb:YAG, and Cr^{4+}:YAG crystals used in the experiments are shown in Table 2.

3. EXPERIMENTAL SETUP

The schematic diagram of the experimental setup for the laser diode pumped passively *Q*-switched microchip laser with C3 by sandwiching a Cr,Yb:YAG crystal between Yb:YAG crystal and Cr^{4+}:YAG crystal is shown in Fig. 2. The doping concentration of Yb^{3+} ions in Yb:YAG crystal is 10 at. %, and thickness of the Yb:YAG crystal is 1.2 mm. One of the Yb:YAG crystal surfaces is coated with anti-reflection (AR) at 940 nm and high reflection (HR) at 1030 nm to act as a rear cavity mirror of the laser, and another surface is coated with anti-reflection at 1030 nm to reduce the intracavity loss. The thickness of the Cr,Yb:YAG crystal is 0.5 mm; the doping concentration of Yb^{3+} ions in the Cr,Yb:YAG crystal is 10 at. %; and the initial transmission of the Cr,Yb:YAG crystal is 94%. The thickness of the Cr^{4+}:YAG crystal is 0.5 mm, and the initial transmission of the Cr^{4+}:YAG crystal is 95%. Both the Cr,Yb:YAG crystal and the Cr^{4+}:YAG crystal are uncoated. A 2-mm-thick BK7 glass plane-parallel mirror with 60% reflection was used as an output coupler (OC). The Yb:YAG crystal, Cr,Yb:YAG crystal, and Cr^{4+}:YAG crystal as well as an OC were mounted in the middle of two copper blocks. The experimental setups for laser diode pumped passively *Q*-switched microchip lasers with C1 and C2 were similar to that of passively *Q*-switched microchip lasers with C3. C1 was a combination of a closely contacted Yb:YAG crystal and Cr^{4+}:YAG crystal, and C2 was a combination of a closely contacted Yb:YAG crystal and Cr,Yb:YAG crystal. A fiber-coupled 940 nm continuous-wave laser diode with a core diameter of 200 μm and numerical aperture of 0.22 was used as the pump source. Two focus lenses with 8 mm focal length were used to collimate and focus the pump beam on the rear surface of the Yb:YAG crystal. The focused pump beam diameter is 100 μm after the collimating and focus lens. The experiment was carried out at room temperature without an active cooling system. The average output power was measured with a Thorlabs PM200 power meter. The laser emitting spectra of the lasers were measured with an Anritsu optical spectral analyzer (MS9740A). The laser pulse characteristics were detected with a 5 GHz InGaAs photo-diode and recorded with a 6 GHz bandwidth Tektronix digital phosphor oscilloscope (TDS6604).

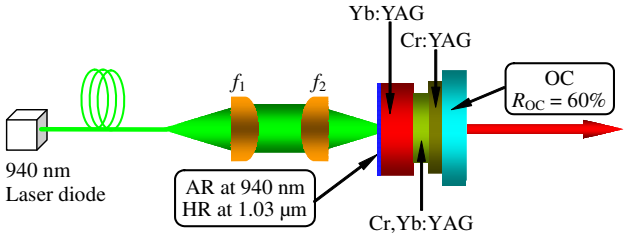

Fig. 2. Schematic diagram of experimental setup for laser diode pumped passively *Q*-switched microchip laser with C3 combination.

4. RESULTS AND DISCUSSION

The average output power of passively *Q*-switched microchip lasers as a function of the incident pump power for C1, C2, and C3 is shown in Fig. 3. The incident pump power thresholds are 2.1, 2.3, and 1.6 W for C1, C2, and C3, respectively.

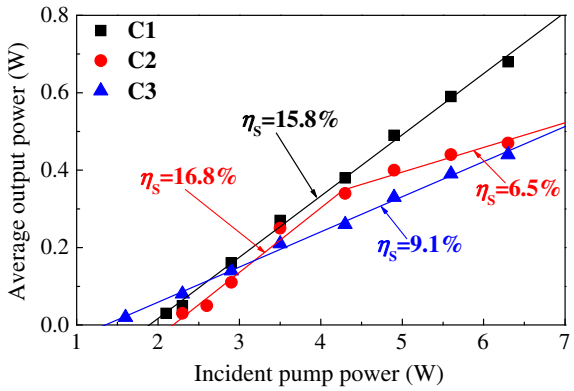

Fig. 3. Average output power of passively Q-switched microchip lasers as a function of the incident pump power for different equivalent composite crystals: C1, C2, and C3. The solid lines are linear fits of the experimental data.

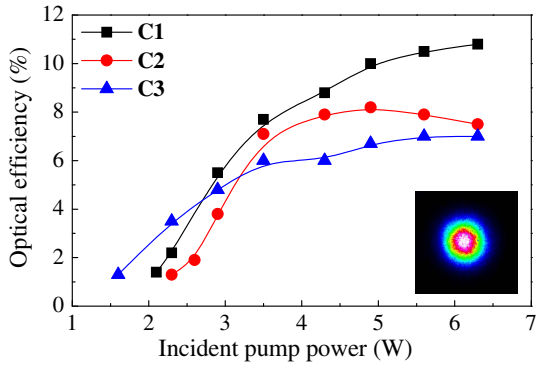

Fig. 4. Optical efficiency of passively Q-switched microchip lasers as a function of the incident pump power for different equivalent Yb:YAG/Cr^{4+}:YAG composite crystals: C1, C2, and C3. Inset shows the laser beam profile for a passively Q-switched microchip laser with a C3 combination at the incident pump power of 6.3 W.

The lowest incident pump power threshold of a passively Q-switched microchip laser with a C3 combination may be caused by the increased modulation of the saturable absorber for the intracavity laser intensity. The average output power increases linearly with the incident pump power for different combinations. The slope efficiencies (η_s) are 15.8%, 16.8%, and 9.1% for C1, C2, and C3 when the incident pump power is above the incident pump power threshold. The slope efficiency of a passively Q-switched microchip laser for C2 drops to 6.5% when the incident pump power is higher than 4.3 W, which may be caused by the losses introduced by the defects in the Cr,Yb:YAG crystal and the absorption of the Cr,Yb:YAG crystal at pump wavelength, resulting in a severe thermal effect. The maximum average output power of 0.68 W is obtained for C1 when the incident pump power is 6.3 W with a corresponding optical efficiency of 10.8%. The maximum average output power is decreased to 0.47 W and 0.44 W for C2 and C3, respectively, when the incident pump power is 6.3 W, and the corresponding optical efficiencies are 7.5% and 7%, respectively. Owing to the absorption of the Cr,Yb:YAG crystal at the pump wavelength of 940 nm and defects introduced in the Cr,Yb:YAG crystal, a similar phenomenon is also observed in a laser diode pumped Yb:YAG/Cr,Yb:YAG self-Q-switched microchip laser [16] and in a laser diode pumped Yb:YAG/Cr, Yb:YAG self-Q-switched laser with a 70-mm-long cavity [17]. The decrease of the optical efficiency for C2 is caused by high intracavity loss with a Cr,Yb:YAG crystal as a saturable absorber introducing more defects. The further decrease of the optical efficiency for C3 is caused by the high intracavity loss induced by the low initial transmission of C3 with both the Cr,Yb:YAG crystal and Cr^{4+}:YAG crystal as saturable absorbers, and the reflecting losses of the interfaces in the C3 combination. Compared with a Yb:YAG crystal, the lattice distortions and self-absorption at 1030 nm of the Cr,Yb:YAG crystal are severe; therefore, the Cr,Yb:YAG crystal is highly sensitive to thermal effects. Heat accumulating in the Cr,Yb:YAG interface layer leads to severe thermal effects and decreases the optical efficiency of the Yb:YAG/Cr, Yb:YAG/Cr^{4+}:YAG passively Q-switched microchip laser.

The Cr,Yb:YAG interface layer formed in the Yb:YAG/Cr^{4+}:YAG composite crystal also has a negative effect on the optical efficiency of passively Q-switched microchip lasers. The optical efficiency of passively Q-switched microchip lasers as a function of the incident pump power for C1, C2, and C3 is shown in Fig. 4. The optical efficiency for C1 increases quickly with the incident pump power when the incident pump power is less than 3.5 W. Next, the optical efficiency increases slowly with further increases in the incident pump power for C1. The highest optical efficiency of 10.8% was obtained when the available incident pump power of 6.3 W was applied. The optical efficiency for C3 increases with the incident pump power when the incident pump power is less than 3.5 W. Next, the optical efficiency increases slowly with further increases in the incident pump power, and the optical efficiency tends to be saturated when the incident pump power is higher than 5.5 W. The highest optical efficiency of 7.5% for C3 was achieved at the available incident pump power of 6.3 W. The variation of the optical efficiency for C2 with the incident pump power is different from those for C1 and C3. The optical efficiency increases with the incident pump power when it is lower than 4.8 W and then decreases with a further increase of the incident pump power. There is an optimal incident pump power, 4.8 W, for achieving the highest optical efficiency for C2. The saturation of optical efficiency with the incident pump power for C2 is caused by high pump power intensity, which depletes the ground state population of Yb^{3+} ions. The thermal effect becomes severe with the further increase of the incident pump power; therefore, the optical efficiency is decreased. It is clearly shown in Fig. 4 that the performance of passively Q-switched microchip lasers with Cr,Yb:YAG interface layers (C2 and C3) is worse than that without the Cr,Yb:YAG interface layer (C1). The formation of the Cr,Yb:YAG interface layer in the Yb:YAG/Cr^{4+}:YAG composite crystal does not degrade the laser beam quality. The perfect TEM_{00} laser mode was observed in a passively Q-switched microchip laser with a C3 combination, as shown in the inset of Fig. 4. Moreover, the beam quality M^2 was measured to be <1.3, and near-diffraction-limited laser beam quality was achieved

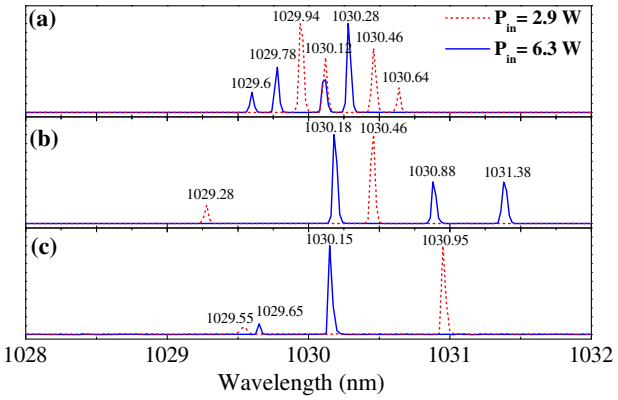

Fig. 5. Typical laser emitting spectra of a passively Q-switched microchip laser at $P_{in} = 2.9$ W and $P_{in} = 6.3$ W for different equivalent composite crystals (a) C1, (b) C2, and (c) C3.

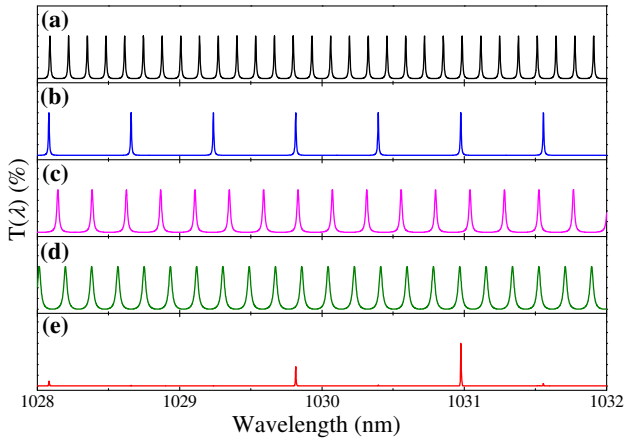

Fig. 6. (a) Resonant modes in a passively Q-switched microchip laser with a C3 combination and transmittance curves of (b) 2-mm-thick BK7 glass output coupler, (c) 0.5-mm-thick Cr,Yb:YAG or Cr^{4+}:YAG, (d) 1.2-mm-thick Yb:YAG, and (e) their transmittance product.

in a passively Q-switched microchip laser with the C3 combination.

Because the cavity lengths in the passively Q-switched microchip laser experiments are at the millimeter level and the emission bandwidth of Yb:YAG crystals and Cr,Yb:YAG crystals is about 9 nm, the passively Q-switched microchip lasers with these three different equivalent composite crystals oscillate in multi-longitudinal-mode. Typical laser emitting spectra of passively Q-switched microchip lasers at incident pump powers P_{in} of 2.9 and 6.3 W for C1, C2, and C3 are shown in Fig. 5. The free spectral ranges (FSR) of passively Q-switched microchip lasers for C1, C2, and C3 are 0.17, 0.17, and 0.13 nm, respectively, which are predicted by $\Delta\lambda_c = \lambda^2/2L_c$ [18], where L_c is the optical cavity length and λ is the laser wavelength. Figure 5(a) shows that four longitudinal modes oscillate in a passively Q-switched microchip laser for C1 at $P_{in} = 2.9$ W and $P_{in} = 6.3$ W. The separation between each longitudinal mode is measured to be about 0.16 and 0.34 nm, which are in good agreement with FSR by taking account into the mode competition effect. Figure 5(b) shows that two longitudinal modes oscillate in a passively Q-switched microchip laser for C2 at $P_{in} = 2.9$ W, and the mode separation between two modes is about 1.18 nm, which is 7 times that of its FSR. Three longitudinal modes oscillate at $P_{in} = 6.3$ W for C2, and the separation between longitudinal modes is measured to be about 0.5 and 0.7 nm. Figure 5(c) shows that two longitudinal modes oscillate in a passively Q-switched microchip laser for C3 at $P_{in} = 2.9$ W, and the separation between the two modes is 1.4 nm (about 10 times that of the FSR). Two-longitudinal-mode oscillation is kept with the increase in the incident pump power. The separation of two longitudinal modes is 0.5 nm at the incident pump power of 6.3 W. The mode separation of passively Q-switched microchip lasers for C2 and C3 are much wider than their FSRs. In addition, the number of longitudinal modes of passively Q-switched microchip lasers for C2 and C3 are less than that of passively Q-switched microchip lasers for C1. The mode selection caused by the Cr,Yb:YAG interface layer suppresses some potential output longitudinal modes and results in the decrease of the longitudinal mode number and the widening of the longitudinal mode separation.

Because the laser crystals and the OC have diffraction losses on their incident surfaces, each of them acts as an intracavity etalon and has the ability to select longitudinal modes. The transmittance of each etalon can be calculated by the following equation:

$$T = \left[1 + \frac{4r}{(1-r)^2}\sin^2\left(\frac{\delta}{2}\right)\right]^{-1}, \tag{3}$$

where r is the reflectivity of the crystal's surface, and δ is the phase difference. Figure 6 shows the intracavity resonant modes and the transmittance curves of the Yb:YAG crystal, Cr,Yb:YAG crystal, Cr^{4+}:YAG crystal and the OC in passively Q-switched microchip laser for C3 and their transmittance product at the incident pump power of 2.9 W. Potential output longitudinal modes at a wavelength with high transmittance are easy to oscillate. The transmittance product shown in Fig. 6(e) is in good agreement with the experimental result shown in Fig. 5(c) at the incident pump power of 2.9 W.

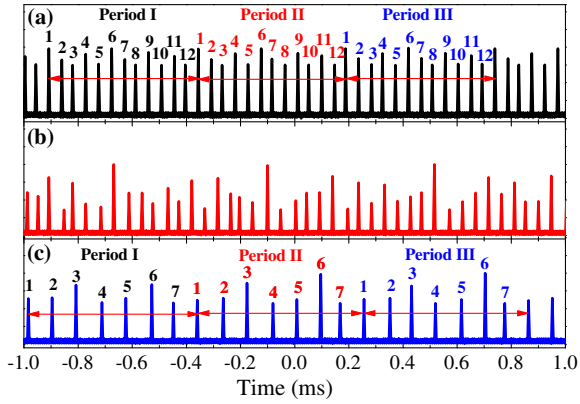

Fig. 7. Laser pulse trains of a passively Q-switched microchip laser for different equivalent composite crystals (a) C1, (b) C2, and (c) C3.

Figure 7 shows the typical laser pulse trains of passively Q-switched microchip lasers for three different equivalent composite crystals at the incident pump power of 6.3 W. A stable laser pulse train with period-12 pulsation is obtained for a passively Q-switched microchip laser with the C1 combination. For a passively Q-switched microchip laser with the C3 combination, a stable laser pulse train with period-7 pulsation is observed. The laser pulse train does not exhibit any periodicity and is unstable for a passively Q-switched microchip laser with the C2 combination. To estimate the laser pulse periodicity stability, we calculate standard deviation of each pulse in the three periods as shown in Figs. 7(a) and 7(c) and choose the maximum standard deviation to estimate the periodical amplitude fluctuation. The periodical amplitude fluctuation of laser pulse trains in passively Q-switched microchip lasers for C1 and C3 is 0.73% and 7.2%, respectively. It is well known that each single-longitudinal mode corresponds with an individual laser pulse. However, because the gain and loss of different longitudinal modes are different, the intensities of pulse energy and the generating time for any individual laser pulse vary with different longitudinal modes. Thus, the total laser pulse trains of passively Q-switched microchip lasers may exhibit periodical pulsation, and time jitters may appear between laser pulse trains. The time jitter of laser pulse trains of passively Q-switched microchip lasers for C1, C2, and C3 is estimated to be 8.2%, 15.8%, and 10.7%, respectively. The laser pulses of passively Q-switched microchip lasers with a Cr,Yb:YAG interface layer are more unstable than those without a Cr,Yb:YAG interface layer, which may be caused by severe thermal effect and mode competition induced by the Cr,Yb:YAG interface layer.

The repetition rate of passively Q-switched microchip lasers for C1, C2, and C3 as a function of the incident pump power is shown in Fig. 8. The repetition rate increases linearly with the incident pump power for C1, C2, and C3. The increase ratio of the repetition rate with the incident pump power is 5 kHz/W for C1 and C2. The highest repetition rate of 21.8 kHz was obtained at the incident pump power of 6.3 W for C1. The increase ratio of the repetition rate with the incident pump power decreases to 2.3 kHz/W for C3. The repetition rate was 11.4 kHz for C3 at the available incident pump power of 6.3 W. The decrease of the repetition rate for C3 is attributed to the low initial transmission of the saturable absorber when the Cr,Yb:YAG and Cr^{4+}:YAG crystals are used simultaneously.

The pulse width for C1 and C2 was kept nearly unchanged with increases in the incident pump power. The pulse width is about 1.1 ns for C1 and C2. The pulse width increases slightly from 0.8 to 1.05 ns with the incident pump power for C3. The short pulse width for C3 is attributed to the low initial transmission of the saturable absorber in the C3 combination with the Cr,Yb:YAG and Cr^{4+}:YAG crystals as saturable absorbers simultaneously. The initial transmission of the C3 combination is about 90%, which is lower than that of the Cr,Yb:YAG crystal (94%) and that of the Cr^{4+}:YAG crystal (95%) used in the experiments. Therefore, short pulse width is achieved in a passively Q-switched microchip laser with the C3 combination.

The pulse energy and peak power of passively Q-switched microchip lasers as a function of the incident pump power for C1, C2, and C3 are shown in Figs. 9 and 10, respectively. The pulse energy increases slowly with incident pump power when the incident pump power is <4.3 W for C1, C2, and C3 and then tends to be constant with further increases in the incident pump power. This is caused by the nonlinear effect of the

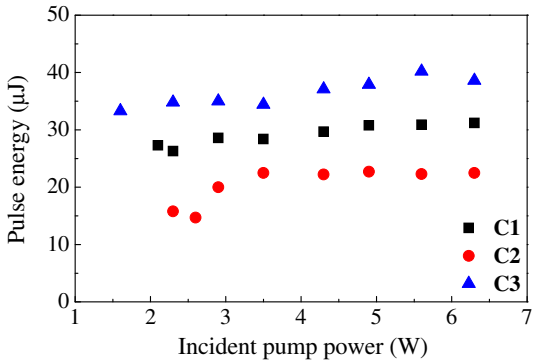

Fig. 9. Pulse energy of passively Q-switched microchip lasers as a function of the incident pump power for different equivalent composite crystals C1, C2, and C3.

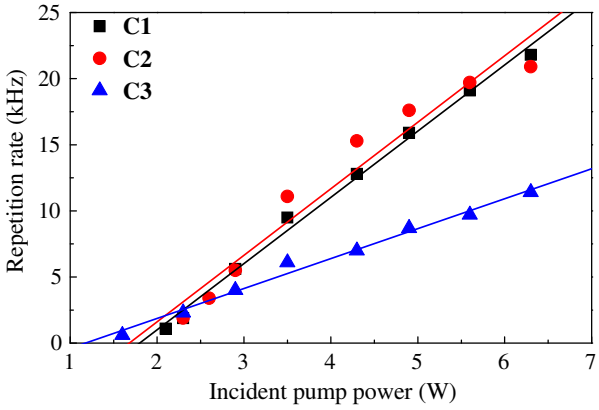

Fig. 8. Repetition rate of passively Q-switched microchip lasers as a function of the incident pump power for different equivalent composite crystals C1, C2, and C3.

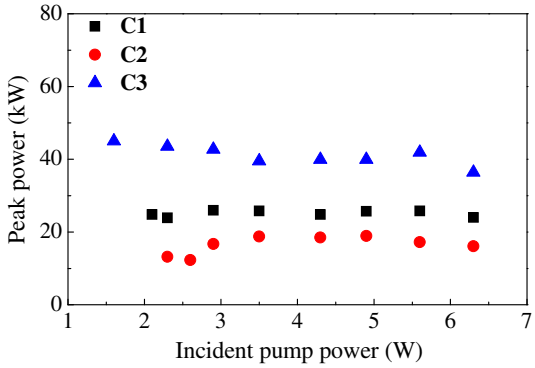

Fig. 10. Peak power of passively Q-switched microchip lasers as a function of the incident pump power for different equivalent composite crystals C1, C2, and C3.

saturable absorber with laser intensity in the laser cavity. The intracavity laser intensity increases with the incident pump power, and the saturable absorber tends to be saturated at high incident pump power. When the intensity of the intracavity laser is high enough, the saturable absorber is fully bleached, the stored energy is fully extracted, and pulse energy is kept constant. The highest pulse energy was achieved in a passively *Q*-switched microchip laser for the C3 combination under the same incident pump power. The pulse energy of a passively *Q*-switched microchip laser with C1 varies from 26.3 to 31.2 μJ with the incident pump power, and its peak power varies between 23.9 and 26 kW. For a passively *Q*-switched microchip laser with C2, the pulse energy varies between 14.7 and 22.5 μJ, and the peak power fluctuates between 12.3 and 18.9 kW. It is clear that the pulse energy and peak power of a passively *Q*-switched microchip laser with C1 are much higher than those of a passively *Q*-switched microchip laser with C2. This may also be attributed to the thermal and self-absorption effects induced by the Cr,Yb:YAG interface layer. High pulse energy and high peak power are generated in a passively *Q*-switched microchip laser with C3, as shown in Figs. 9 and 10. The high pulse energy and high peak power generated in a passively *Q*-switched microchip laser with the C3 combination is caused by the increase of the modulation depth of the saturable absorber.

Although formation of a Cr,Yb:YAG codoped interface layer in a Yb:YAG/Cr^{4+}:YAG composite crystal has degraded the average output power and the optical efficiency, the good beam quality is still kept in a passively *Q*-switched microchip laser with the C3 combination. The stable laser pulses with high beam quality could be achieved by choosing suitable parameters in fabricating Yb:YAG/Cr^{4+}:YAG composite crystal for a passively *Q*-switched microchip laser.

5. CONCLUSIONS

The effect of a Cr,Yb:YAG interface layer on the performance of a Yb:YAG/Cr^{4+}:YAG composite crystal passively *Q*-switched microchip laser has been investigated by sandwiching a thin piece of Cr,Yb:YAG crystal between the Yb:YAG crystal and Cr^{4+}:YAG crystal. The Cr,Yb:YAG interface layer degrades average output power and optical-to-optical efficiency of a Yb:YAG/Cr^{4+}:YAG composite crystal passively *Q*-switched microchip laser. The laser pulse train stability is also degraded by a Cr,Yb:YAG interface layer between the Yb:YAG crystal and Cr^{4+}:YAG crystal. Moreover, a Cr,Yb:YAG interface layer also results in a strong mode competition between longitudinal modes in a passively *Q*-switched microchip laser. The longitudinal mode number is decreased, and separation between longitudinal modes is widened with a Cr,Yb:YAG interface layer in a Yb:YAG/Cr^{4+}:YAG composite crystal. The intensities and the number of the longitudinal modes in a Yb:YAG/Cr^{4+}:YAG composite crystal passively *Q*-switched microchip laser are more easily controlled with suitable selected pumping intensity, which is beneficial for highly stable laser pulse generation in passively *Q*-switched microchip lasers. Our work provides a new approach for designing Yb:YAG/Cr^{4+}:YAG composite crystals for highly stable, high peak power generation in passively *Q*-switched microchip lasers.

Funding. National Natural Science Foundation of China (NSFC) (61275143), (61475130).

Acknowledgment. J. Xu would like to thank Dr. X. L. Wang, D. M. Chen, and Mr. G. Y. Wang for their help in experiments and discussion.

REFERENCES

1. Y. T. Chang, Y. P. Huang, K. W. Su, and Y. F. Chen, "Comparison of thermal lensing effects between single-end and double-end diffusion-bonded Nd:YVO_4 crystals for $^4F_{3/2}$–>$^4I_{11/2}$ and $^4F_{3/2}$–>$^4I_{13/2}$ transitions," Opt. Express **16**, 21155–21160 (2008).
2. J. J. Zayhowski and C. Dill, "Diode-pumped passively *Q*-switched picosecond microchip lasers," Opt. Lett. **19**, 1427–1429 (1994).
3. J. Dong, K. I. Ueda, A. Shirakawa, H. Yagi, T. Yanagitani, and A. A. Kaminskii, "Composite Yb:YAG/Cr^{4+}:YAG ceramics picosecond microchip lasers," Opt. Express **15**, 14516–14523 (2007).
4. N. Pavel, M. Tsunekane, and T. Taira, "Composite, all-ceramics, high-peak power Nd:YAG/Cr^{4+}:YAG monolithic micro-laser with multiple-beam output for engine ignition," Opt. Express **19**, 9378–9384 (2011).
5. J. Dong, Y. Y. Ren, G. Y. Wang, and Y. Cheng, "Efficient laser performance of Yb:$Y_3Al_5O_{12}$/Cr^{4+}:$Y_3Al_5O_{12}$ composite crystals," Laser Phys. Lett. **10**, 105817 (2013).
6. N. Belghachem and J. Mlynczak, "Comparison of laser generation in thermally bonded and unbonded Er^{3+}, Yb^{3+}:glass/Co^{2+}:$MgAl_2O_4$ microchip lasers," Opt. Mater. **46**, 561–564 (2015).
7. J. Dong, P. Z. Deng, and J. Xu, "The growth of Cr^{4+}, Yb^{3+}:yttrium aluminum garnet (YAG) crystal and its absorption spectra properties," J. Cryst. Growth **203**, 163–167 (1999).
8. J. Dong, A. Shirakawa, S. Huang, Y. Feng, K. Takaichi, M. Musha, K. Ueda, and A. A. Kaminskii, "Stable laser-diode pumped microchip sub-nanosecond Cr, Yb:YAG self-*Q*-switched laser," Laser Phys. Lett. **2**, 387–391 (2005).
9. J. Dong and P. Z. Deng, "The effect of Cr concentration on emission cross-section and fluorescence lifetime in Cr, Yb:YAG crystal," J. Lumin. **104**, 151–158 (2003).
10. J. Dong and P. Z. Deng, "Temperature dependent emission cross-section and fluorescence lifetime of Cr, Yb:YAG crystals," J. Phys. Chem. Solids **64**, 1163–1171 (2003).
11. J. Dong, K. I. Ueda, H. Yagi, and A. A. Kaminskii, "Laser-diode pumped self-*Q*-switched microchip lasers," Opt. Rev. **15**, 57–74 (2008).
12. R. D. Shannon and C. T. Prewitt, "Effective ionic radii in oxides and fluorides," Acta Crystallogr. Sect. B **25**, 925–946 (1969).
13. J. P. Hollingsworth, J. D. Kuntz, and T. F. Soules, "Neodymium ion diffusion during sintering of Nd:YAG transparent ceramics," J. Phys. D **42**, 052001 (2009).
14. K. Fujioka, A. Sugiyama, Y. Fujimoto, J. Kawanaka, and N. Miyanaga, "Ion diffusion at the bonding interface of undoped YAG/Yb:YAG composite ceramics," Opt. Mater. **46**, 542–547 (2015).
15. H. Yagi, K. Takaichi, K. Ueda, Y. Yamasaki, T. Yanagitani, and A. A. Kaminskii, "The physical properties of composite YAG ceramics," Laser Phys. **15**, 1338–1344 (2005).
16. Y. Cheng, J. Dong, and Y. Y. Ren, "Enhanced performance of Cr, Yb:YAG microchip laser by bonding Yb:YAG crystal," Opt. Express **20**, 24803–24812 (2012).
17. J. Y. Zhou, J. Ma, J. Dong, Y. Cheng, K. Ueda, and A. A. Kaminskii, "Efficient, nanosecond self-*Q*-switched Cr, Yb:YAG lasers by bonding Yb:YAG crystal," Laser Phys. Lett. **8**, 591–597 (2011).
18. W. Koechner, *Solid State Laser Engineering* (Springer-Verlag, 1999).